energies

MDPI

Article

Short-Term Wind Power Forecasting Based on OMNIC and Adaptive Fractional Order Generalized Pareto Motion Model

Fan Cai [1,2], Dongdong Chen [1,*], Yuesong Jiang [1,3] and Tongbo Zhu [1,2]

[1] School of Electronic and Electrical Engineering, Minnan University of Science and Technology, Quanzhou 362700, China; caifan202208@163.com (F.C.); yuesongjiang@vip.sina.com (Y.J.); ztb2018@xmu.edu.cn (T.Z.)
[2] Key Laboratory of Industrial Automation Control Technology and Application of Fujian Higher Education, Quanzhou 362700, China
[3] School of Electronic and Information Engineering, Beihang University, Beijing 100000, China
* Correspondence: 3090104956@zju.edu.cn

Abstract: With the rapid development of renewable energy, accurately forecasting wind power is crucial for the stable operation of power systems and effective energy management. This paper proposes a short-term wind power forecasting method based on the Orthogonalized Maximal Information Coefficient (OMNIC) combined with an Adaptive fractional Generalized Pareto motion (fGPm) model. The method quantifies the influence of meteorological factors on wind power prediction and identifies the optimal set and number of influencing factors. The model accounts for long-range dependence (LRD) in time series data and constructs an uncertainty model using the properties and parameters of the fractional generalized Pareto distribution (GPD), significantly improving prediction accuracy under nonlinear conditions. The proposed approach was validated using a real dataset from a wind farm in northwest China and compared with other models such as Convolutional Neural Network-Long Short-Term Memory (CNN-LSTM) and Convolutional Neural Network-Gated Recurrent Unit (CNN-GRU). Results show that the adaptive fGPm model reduces RMSE by 0.448 MW and 0.466 MW, MAPE by 6.936% and 9.702%, and achieves an average R^2 of 0.9826 compared to CNN-GRU and CNN-LSTM. The improvement is due to the dynamic adjustment to data trends and effective use of LRD features. This method provides practical value in improving wind power prediction accuracy and addressing grid integration and regulation challenges.

Keywords: wind power forecasting; orthogonalized maximal information coefficient; adaptive fractional generalized pareto motion model; LRD; uncertainty modeling

Citation: Cai, F.; Chen, D.; Jiang, Y.; Zhu, T. Short-Term Wind Power Forecasting Based on OMNIC and Adaptive Fractional Order Generalized Pareto Motion Model. *Energies* **2024**, *17*, 5848. https://doi.org/10.3390/en17235848

Academic Editor: Davide Astolfi

Received: 11 October 2024
Revised: 10 November 2024
Accepted: 20 November 2024
Published: 22 November 2024

1. Introduction

The Wind energy, as one of the most critical renewable energy sources, plays a significant role in the planning and scheduling of power systems. However, the uncertainty and random fluctuations of wind power not only affect the stability of power generation but also pose challenges to grid security and data processing efficiency [1]. The challenge of wind power forecasting lies in its inherent uncertainty and random fluctuations, which affect wind power output, energy integration, and forecasting accuracy. Additionally, the mismatch between wind power and energy demand increases the complexity of grid integration, necessitating more reliable forecasting methods [2].

Recent studies have shown that the combination of blockchain technology and machine learning can enhance the data security and monitoring capabilities of distributed energy systems. For example, Faheem, M. et al. [3] improved the ability to respond to network attacks by using Industrial Wireless Sensor Networks (IWSNs) to monitor wind farm events, thereby ensuring the communication security of renewable energy. Additionally, Faheem, M. et al. [4] employed deep learning and LSTM models to identify network attacks, enhancing the real-time detection and response capabilities of wind power systems, thereby

improving the accuracy and response speed of wind power forecasts. Therefore, in the face of wind power uncertainty and data security issues, increasing research focuses not only on improving the accuracy of forecasting models but also on ensuring the security and efficiency of data. This paper combines the OMNIC to analyze the correlation between meteorological features and wind power and proposes a forecasting method based on the Adaptive fGPm model, aiming to improve the accuracy and robustness of forecasts while meeting real-time requirements.

In recent years, new technologies have continually emerged in the field of wind power forecasting. For instance, Zhao, P. et al. [5] proposed a multi-step multivariate residential load forecasting model based on a spatiotemporal graph attention mechanism, which improves prediction accuracy by modeling spatiotemporal correlations. Zhang, Y. et al. [6] proposed a wind power forecasting system that combines data augmentation and algorithm improvements, which effectively enhanced the stability and accuracy of wind power forecasting. Although these methods have been successful in other fields, their application in wind power forecasting still requires further exploration. Therefore, this paper proposes a wind power forecasting method that combines OMNIC with the Adaptive fGPm model, aiming to address the long-range dependence and nonlinearity characteristics of wind power data.

To tackle this issue, current research primarily focuses on improving feature input and constructing precise models to enhance the accuracy and reliability of wind power forecasting. In terms of feature extraction, researchers utilize feature processing techniques to provide models with richer feature information. For instance, Ju, Y. et al. [7] constructed a novel feature set by analyzing the characteristics of time series raw data from wind farms and neighboring wind farms, proposing the use of CNN to extract information from input data. Zhao, Y.B. et al. [8] were the first to apply the NeuralProphet model to decompose wind power time series data, accurately capturing the complex nonlinear patterns hidden within wind power time series.

In the realm of model construction, machine learning and deep learning have made remarkable progress as the primary statistical models in the field of wind power forecasting in recent years [9–12]. Liao, S.L. et al. [13] introduced a Light Gradient Boosting Machine (LightGBM) model with strong nonlinear fitting capabilities, which can fully exploit the valuable information in historical wind power operation data. Wang, Y.S. et al. [13] proposed a wind farm output power forecasting model based on the Sliding Time Window (TSW) and LSTM [14], effectively fitting the output power curve of the wind farm and achieving accurate wind power prediction. Yu, C.Q. et al. [15] combined Graph Attention Networks (GAT), GRU, and Temporal Convolutional Networks (TCN) to effectively extract features from wind power time series data, significantly improving the model's accuracy and robustness. Yang Guohua et al. [16] proposed a short-term wind power forecasting model based on Complementary Ensemble Empirical Mode Decomposition-Sample Entropy (CEEMD-SE),CNN, and LSTM-GRU [17], demonstrating that the model effectively enhanced forecasting accuracy, reducing the error by 15.06%. However, deep learning models require the setting of numerous parameters, and hyperparameters determined by expert experience often differ from the optimal parameters needed by the model. Moreover, as the volume of data increases, especially when the model becomes overly complex, more computational resources and training time are required.

As a result, accurate wind power forecasting has become a key solution to the issues associated with wind power grid integration [18]. Current methods have the following limitations:

(1) Data and model overfitting: Deep learning models and others require large amounts of data, which can lead to overfitting and poor generalization to new data.
(2) Lack of Long-Range Dependence (LRD): Many models fail to capture the long-range dependence in wind power time series data, affecting long-term forecasting accuracy.
(3) Difficulty in nonlinear modeling: Traditional methods struggle to effectively capture the nonlinear characteristics of wind power time series, impacting forecasting accuracy.

(4) High computational complexity: Complex models, especially deep learning models, require significant computational resources and training time, which can hinder real-time forecasting applications.

To further address these issues, this paper employs the OMNIC to analyze the correlation between meteorological features and wind power for feature extraction [19], which effectively meets the timeliness requirements of wind power forecasting tasks. Considering the long-range dependence characteristics of wind power [20,21]. an Adaptive fGPm forecasting model is proposed to cope with the randomness and volatility of wind energy [22,23]. This approach builds upon the strengths of existing research while addressing their shortcomings, such as the inability to model LRD effectively or adapt dynamically to data changes. To verify the practicality and effectiveness of the proposed method, a case analysis of wind power data from a wind farm in Northwest China is conducted [24]. Two scenarios are selected for the experiment: one with significant meteorological feature fluctuations in winter from 12 December 2019, 7:00 to 14 December 2019, 19:00 (Case 1), and another with smaller fluctuations in summer from 12 July 2019, 7:00 to 14 July 2019, 19:00 (Case 2), serving as historical feature data [25,26]. These data are used to predict the optimal power change trends of wind power within the next 12, 24, 36, and 48 steps. Compared with previous methods, the model shows higher precision in power forecasting.

The main motivations and objectives of this paper are as follows:

(1) Motivation: To address the uncertainty and complexity in wind power forecasting, particularly the correlation and LRD characteristics of wind power, as well as the nonlinear relationships between meteorological features and wind power.
(2) Objective: To capture the nonlinear correlation between meteorological data and wind power using the OMNIC, optimize feature inputs, and fully explore the correlation between wind turbine features and wind power output, thereby improving the timeliness and accuracy of wind power forecasting.
(3) Objective: To propose an Adaptive fGPm iterative differential forecasting model that considers the LRD characteristics in wind power time series data, and more accurately predicts unstable stochastic processes by accounting for past, present, and future states.

The main contributions of this paper are as follows:

(1) Improved Feature Extraction Method: By using the OMNIC to analyze the correlation between meteorological features and wind power, this paper improves the feature inputs for wind power forecasting, effectively capturing the nonlinear relationships in time series data.
(2) Adaptive fGPm Model: A novel adaptive fGPm model is proposed, integrating long-range dependence characteristics and dynamic parameter adaptation, capable of addressing the randomness and volatility in wind power forecasting, thus providing more accurate predictions.
(3) Innovative Algorithm Design: The proposed Adaptive fGPm iterative differential forecasting model dynamically adjusts the diffusion coefficient, allowing it to automatically adapt to data changes, optimizing system performance, reducing forecasting errors, and enhancing prediction accuracy. This innovative design effectively overcomes the limitations of traditional methods that fail to fully address the complexity and nonlinear relationships in wind power time series.
(4) Validation with Real Data: The method is validated using real wind power data from a wind farm in Northwest China, demonstrating that the model outperforms traditional forecasting models in terms of prediction accuracy.
(5) Practical Application Value: This method improves the accuracy of wind power forecasting, providing a practical solution for wind power grid integration and ensuring the stability of power systems.

Innovation:

(1) Adaptive Feature: The proposed Adaptive fGPm iterative differential forecasting model has the ability to dynamically adjust the diffusion coefficient, enabling it to automatically optimize system performance in response to changes in the environment during the forecasting process.
(2) Effective LRD Modeling: By incorporating long-range dependence characteristics, the model can better handle long-term trends in wind power time series, thus improving forecasting accuracy.
(3) Capturing Nonlinear Relationships: The use of the OMNIC method effectively captures the nonlinear relationships between meteorological features and wind power, significantly enhancing the accuracy of feature inputs.

The structure of this paper is arranged as follows: Section 2 analyzes the input feature variables that affect wind power, introducing the principles and steps of the OMNIC method in data preprocessing [27]. Section 3 discusses the properties and parameters of the fractional-order Generalized Pareto Distribution (fGPD) [28], emphasizing the analysis of the distribution's LRD and heavy-tailed characteristics [29]. Additionally, the mathematical expression of the adaptive fGPm model and its incremental form are introduced, exploring the LRD characteristics of fGPm and the process of generating numerical sequences. Section 4 proposes an adaptive fGPm iterative differential forecasting model based on Langevin-type stochastic differential equations (SDE) [30,31], describing its parameter estimation methods. Section 5 conducts experimental validation using measured wind power data from a wind farm in Northwest China, demonstrating the efficiency and applicability of the model through comparisons with other models [32,33]. Finally, Section 6 summarizes the main research findings of this paper and discusses future research directions.

2. Feature Extraction

Within wind farms, a multitude of factors can influence the power output of wind energy, with meteorological characteristics being the most critical, such as wind speed, direction, temperature, humidity, and air pressure [34,35]. Selecting features based solely on the correlation between two variables may lead to significant redundancy among them [36,37]. In this study, we employ the OMI-Coherence to analyze the correlation between meteorological characteristics and wind power, which more accurately captures the nonlinear relationships between variables [38]. The specific implementation steps are as follows:

Step 1: Define Mutual Information

For a two-dimensional dataset $D = (X, Y)$ composed of variables X and Y, divide the space along each axis into intervals X_0 and Y_0, forming a grid G of size $X_0 \times Y_0$ [39]. Based on the distribution of D/G, the mutual information between X and Y is defined as:

$$I(X,Y) = \sum_{i}^{Y_0} \sum_{j}^{X_0} p(i,j) \log_2 \left(\frac{p(i,j)}{p(i)p(j)} \right) \tag{1}$$

where $p(i,j)$ is the joint probability distribution of X and Y, and $p(i)$ and $p(j)$ are the marginal probability distributions of X and Y, respectively [40].

Step 2: Calculate and Normalize Mutual Information

From the grid G, identify the maximum value of mutual information $I(D, X_0, Y_0)$ as the output. Construct a normalized feature matrix M based on this value [41]. The normalized mutual information matrix M_{IC} for a total sample size of n is given by:

$$M_{IC} = \max_{X_0 Y_0 < B(n)} (M(X_0, Y_0)) M(X_0, Y_0) = \frac{I(D, X_0, Y_0)}{\log_2 \min(X_0, Y_0)} \tag{2}$$

Step 3: Compute OMI-Coherence

For the set of variables $S = \{x_1, x_2, x_3, \cdots, x_n\}$ and the target variable Y, calculate the maximal information coefficient value between the feature information of x_{k+1}, which is independent of the selected variable set S_k, and the target variable Y [42]. This is expressed as:

$$\begin{aligned} O_{\mathrm{MICS}}(x_{k+1}, \mathbf{S}_k) &= \text{OMI-Coherence}\ (x_{k+1}; Y \mid S_k) \\ &= \max_{\text{functions}\ f,g} \frac{I(f(x_i); g(Y))}{\max(H(f(x_i)), H(g(Y)))} \end{aligned} \tag{3}$$

Here, $I(f(x_i); g(Y))$ represents the mutual information between the transformed variables [40].

Step 4: Variable Selection and Ranking

Based on the OMI-Coherence values, select the variable with the highest OMI-Coherence value, then incrementally add other variables according to the ranking rules established [43]. The feature vector selected after the k-th choice is used to construct the final feature sequence:

$$\mathbf{S}_k = \underset{x_k \in S - s_{k-1}}{\operatorname{argmax}} \left(O_{\mathrm{MICS}}(x_k, \mathbf{S}_{k-1}) \right) \tag{4}$$

This approach effectively selects the most relevant features from meteorological characteristics for wind power forecasting, reduces redundancy among features, and enhances the performance of the predictive model.

3. Model Principle

3.1. Properties and Parameter of the Fractional-Order GPD

The GPD [44] serves as an extension of the Pareto distribution, characterized for modeling the tail behavior of probability distributions with heavier tails. Its Probability Density Function (PDF) is:

$$f(x|\mu, \delta, \alpha) = \frac{1}{2\delta} \left[1 + \frac{1}{\alpha\delta} |x - \mu| \right]^{-1-\alpha} \tag{5}$$

In this context, μ represents the location parameter of the distribution, δ denotes the scale parameter, and α signifies the shape parameter [45].

Figure 1 illustrates the GPD with its tail decaying in accordance with a power law. The larger the value of the shape parameter $\alpha \in (0, 2]$, the more pronounced the heavy-tailed nature of the distribution, resulting in a more rapid decrease within the same time frame [46]. Conversely, a smaller α indicates a greater impulsiveness in the sequence, where anomalies occurring further from the central position have a more substantial impact [47].

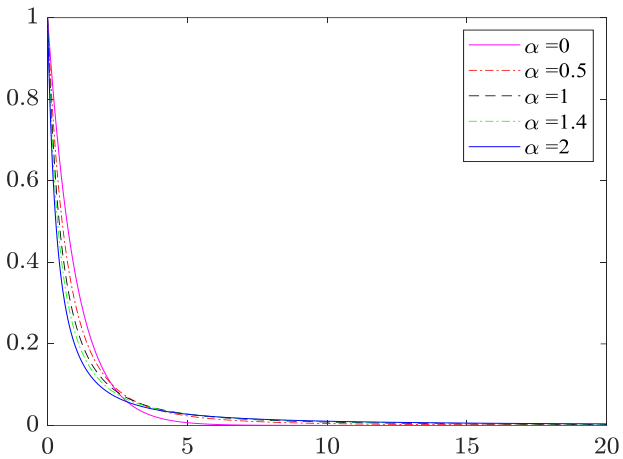

Figure 1. PDF of GPD with Different Shape Parameters.

As shown in Figure 2, the scale parameter δ of the GPD signifies the extent of deviation from the mean. When $\delta \geq 0$ it reflects the dispersion of the distribution around the mean, and in a particular case, it is analogous to the variance of a normal distribution [48].

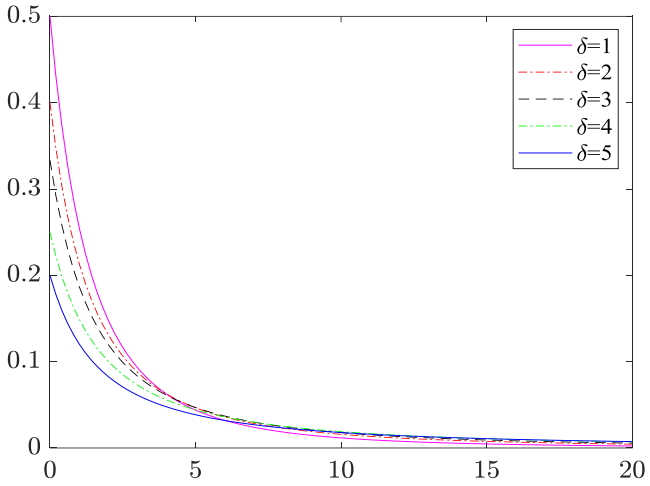

Figure 2. PDF of GPD with Different Scale Parameters.

Hence, if a stochastic process $X(i)$ exhibits power-law decay in its probability distribution, characterizing heavy tails, it will also manifest LRD characteristics in the realm of its autocorrelation function [49].

3.2. fGPm Model and LRD Characteristics

In the literature, a class of fGPm models, founded on stochastic Weyl integrals [50], is defined with the following expression:

$$B_H(t) = \int_{-\infty}^{\infty} \left\{ \begin{array}{l} a\left[(t-s)_+^{H-\frac{1}{2}} - (-s)_+^{H-\frac{1}{2}}\right] + \\ b\left[(t-s)_-^{H-\frac{1}{2}} - (-s)_-^{H-\frac{1}{2}}\right] \end{array} \right\} B(ds) \tag{6}$$

$B_H(t)$ is a fractional Brownian motion with Hurst exponent H, where H is the self-similarity parameter that controls the self-similarity or LRD of the process. $B(ds)$ represents a Gaussian process with mean 0 and variance $|ds|$, which serves as the driving noise in the process. In the Ito process. In which $(x)_+^{H-\frac{1}{2}} = (-x)_-^{H-\frac{1}{2}} = \begin{cases} x, & x > 0 \\ 0, & x \leq 0 \end{cases}$, The term $(t-s)^{H-\frac{1}{2}} - (-s)^{H-\frac{1}{2}}$ represents the self-similarity of the fGPm model. a, b are real constants, which respectively control the volatility and mean of the stochastic process, and satisfy $|a|+|b|>0$. The Hurst index determines the correlation between the past at time t and the future at time s. Its autocorrelation function is given by:

$$R_{B_H}(t,s) = \frac{\Gamma(1-2H)\frac{\cos \pi H}{\pi H}}{(H+1/2)\Gamma(H+1/2)}\left[|t|_{2H}+|s|_{2H}-|t-s|^{2H}\right] \tag{7}$$

The autocorrelation function of the fGPm varies over time, as the characteristics of wind power generation and the impact of multi-dimensional environmental factors on wind power output exhibit non-stationarity in industrially collected data. Consequently, the LRD characteristics of the fGPm model are determined by the relationship between the self-similarity parameter H and α. The larger the product of H and α, the stronger the LRD

characteristics of the fGPm model, leading to a more complex and variable trend in the stochastic sequence. When $0 < H < 0.5$, $B_H(t)$ possesses anti-persistence, indicating that the past correlations of the fGPm model are inversely related to future trends. Conversely, when $f_{\alpha,H}(a,b;t,s)$, the integral kernel function $f_{\alpha,H}(a,b;t,s)$ changes very slowly with the variable s [51], causing the integral of the kernel function to diverge at infinity. This persistent effect endows the fGPm model with LRD characteristics, making it a suitable model for forecasting.

3.3. Generation of Numerical Sequences for fGPm Processes

The central idea of LRD stochastic model forecasting is to generate numerical sequences using stochastic models to approximate the actual wind power random sequences. Compared to other methods, there is an improvement in the length and accuracy of the forecast. The expression of the fGPm model is presented in Equation (8) as follows:

$$P_{H,\alpha}(t) = \int_{-\infty}^{\infty} \left\{ \begin{array}{l} a\left[(t-s)_+^{H-\frac{1}{\alpha}} - (-s)_+^{H-\frac{1}{\alpha}} \right] \\ +b\left[(t-s)_-^{H-\frac{1}{\alpha}} - (-s)_-^{H-\frac{1}{\alpha}} \right] \end{array} \right\} p(ds) \tag{8}$$

The fGPm is defined using the Riemann-Liouville fractional integral [52] as follows:

$$P_{H,a}(t) = \frac{1}{\Gamma\left(H+\frac{1}{2}\right)} \int_0^t (t-\tau)^{H-\frac{1}{2}} p(d\tau) \tag{9}$$

In which $\Gamma(x) = \int_0^{\infty} t^{x-1} e^{-t} dt$ denotes the gamma function, and H represents the calculated Hurst value. By discretizing the increment $P_{H,\alpha}(t)$ of the fGPm model, the model generates a stationary increment sequence, that is, the fractional-order Lévy stable noise sequence $X_{H,\alpha}(t)$ [53], which is expressed as (Equation (10)):

$$X_{H,\alpha}(t) = P_{H,\alpha}(t+1) - P_{H,\alpha}(t) = \int_{-\infty}^{\infty} \left\{ \begin{array}{l} a\left[(t+1-s)_+^{H-1/\alpha} - (-s)_+^{H-1/\alpha} \right] + \\ b\left[(t+1-s)_-^{H-1/\alpha} - (-s)_-^{H-1/\alpha} \right] \end{array} \right\} pds \tag{10}$$

Equation (10) describes the fGPm incremental process, which represents the increment of the fGPm process between the continuous time points t and $t+1$, simulating the dynamic behavior of a time series. The key elements of this incremental process are the power-law functions and the noise process, which control the variation of the time series. $(t+1-s)^{H-1/\alpha} - (-s)^{H-1/\alpha}$ control the long-range dependence (LRD) of the time series. $w_\alpha(s)$ represents the noise component of the process and follows the generalized double Pareto distribution (GPD). Subsequently, integrating or accumulating this noise yields the numerical simulation sequence of the fGPm model, with the expression provided as follows:

$$P_{H,\alpha} = \frac{1}{\Gamma(\alpha+1)} \int_{-\infty}^{\infty} \left\{ \begin{array}{l} a\left[(t+1-s)_+^{H-1/\alpha} - (-s)_+^{H-1/\alpha} \right] + \\ b\left[(t+1-s)_-^{H-1/\alpha} - (-s)_-^{H-1/\alpha} \right] \end{array} \right\} \omega_a(s) ds \tag{11}$$

As illustrated in Figure 3, when $0.5 < H < 1$, it is observable that as the value of α increases, the stochastic fluctuations of the fGPm model become less pronounced and occur more rapidly. This implies a diminishing impulsiveness characterized by heavy tails and sharp peaks, with the LRD properties becoming increasingly evident.

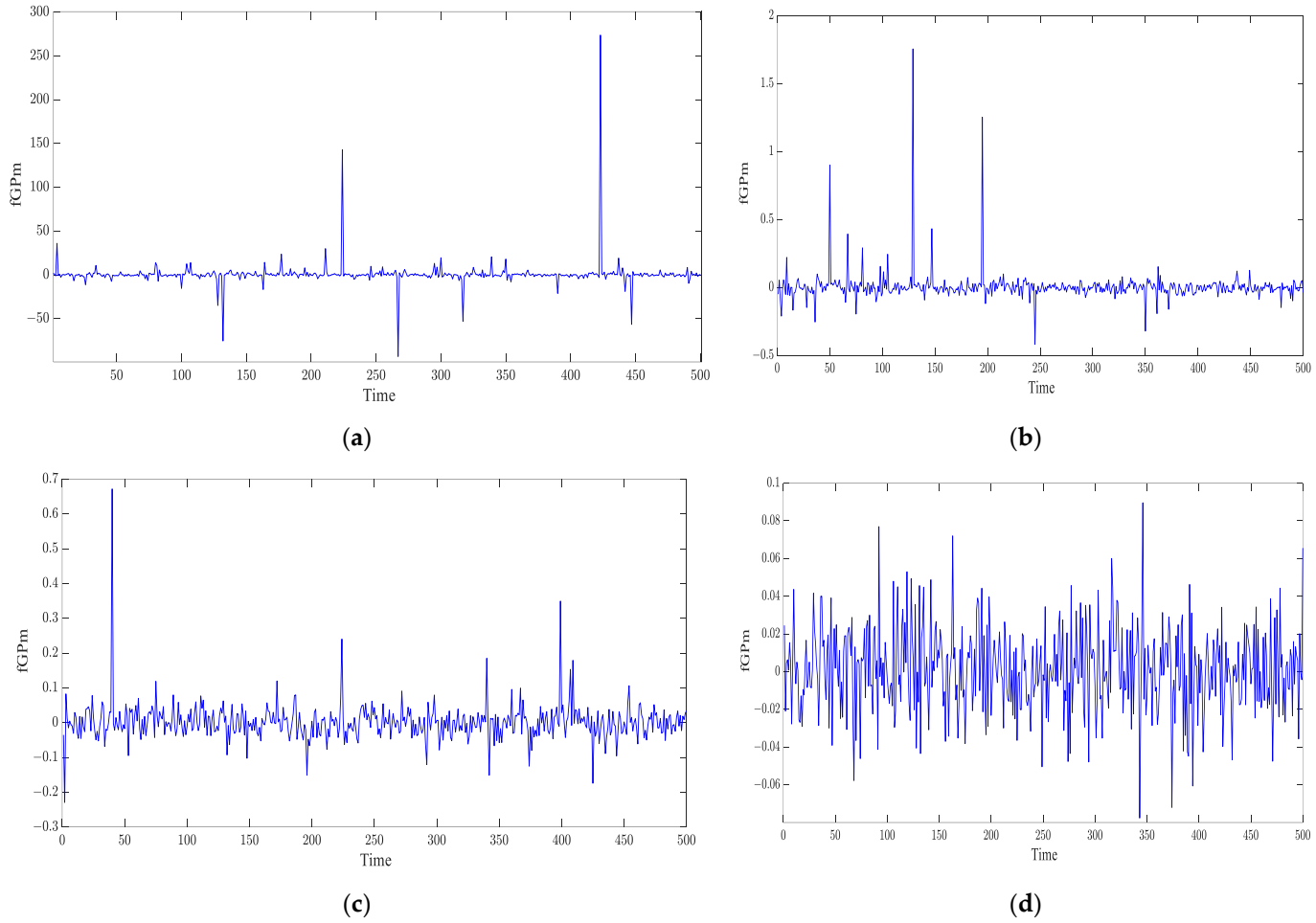

Figure 3. Simulation sequences of the fGPm model under different conditions (**a**) $H = 0.85$, $\alpha = 1.1$; (**b**) $H = 0.85$, $\alpha = 1.4$; (**c**) $H = 0.85$, $\alpha = 1.7$; (**d**) $H = 0.85$, $\alpha = 2$. Time representation in the figure is specified as time steps, where each time step represents the simulated sequence count.

3.4. Establishing an Uncertainty Model with Adaptive fGPm

Uncertainty is a pivotal element in wind power forecasting, predominantly stemming from environmental noises that encompass the random variations of meteorological attributes such as wind speed, direction, and temperature. To capture these uncertainties more precisely, this paper proposes an Adaptive fGPm model featuring a self-adjusting diffusion coefficient. This model is adept at updating the evolution within stochastic processes in a self-adaptive manner, offering a more robust modeling of trend uncertainties for the prediction of wind power.

The definition of the adaptive diffusion coefficient is presented in Equation (12):

$$\sigma_H(t) = \sigma_H(t-1) + \varepsilon \tag{12}$$

In Equation (12), the stochastic sequence $\varepsilon \sim N\left(0, \sigma_\varepsilon^2\right)$ reflects the variations in environmental noise, while σ_ε^2 measures the intensity of randomness. The diffusion coefficient is initialized at 1 and, over time and with the accumulation of data, it will adaptively adjust according to actual observed values.

The general form of the driving process for the Adaptive fGPm model, as presented in [54] (Equation (13)), is expressed as follows:

$$X(t) = \frac{1}{2} X_{H,\alpha}(t) + \sigma_H(t) P_{H,\alpha} \tag{13}$$

4. Forecast Model Construction

4.1. Establishment of Iterative Differential Forecasting Model

A. A. Stanislavsky et al. [55] introduced a FARIMA model incorporating Pareto noise, which serves as a discrete-time analogue of the fractional Langevin equation, accounting for non-Gaussian statistical measures and LRD [56]. Building upon this foundation, this paper further explores the Langevin-type stochastic differential equation driven by the GPD as follows (Equation (14)):

$$dX(t) = b(t, X(t))dt + \delta(t, X(t))dp_a(t) \tag{14}$$

Here, $dp_a(t)$ represents the increment of the Generalized Pareto Motion; replacing $P_{H,a}(t)$ with $P_a(t)$ yields the Langevin-type stochastic differential equation driven by the fGPm as follows (Equation (15)):

$$dX_{H,a}(t) = \mu(t, X_{H,a}(t))dt + \delta(t, X_{H,a}(t))dP_{H,a}(t) \tag{15}$$

In this equation, μ is the expected location parameter and $\delta > 0$. Within the adaptive fGPm framework, the iterative forecasting model is constructed based on incremental modeling. By integrating the discrete form of the fractionalorder Ito process with a differential equation, we derive the iterative differential forecasting model based on the adaptive fGPm model (Equation (16)):

$$P_{H,\alpha}(t+1) = P_{H,\alpha}(t) + \mu P_{H,a}(t)\Delta t + \delta P_{H,a}(t) w_\alpha(t)(\Delta t)^{H-\frac{1}{2}+\frac{1}{\alpha}} \tag{16}$$

where, $0 < H < 1$, to ensure long-term dependence is maintained, and the time step $\Delta t > 0$, to ensure the stability of numerical integration.

4.2. Parameter Estimation of the New Feature Function

The precise estimation of the shape parameter α, the location parameter μ, and the diffusion parameter δ is essential for the construction of the predictive model based on the adaptive fGPm [57]. The Log-Likelihood Estimation (MLE) method is utilized to estimate the specific parameters within the adaptive fGPm model framework [58]. The specific process is as follows:

Step 1: First, define the sample sequence $|x_i|_{i=1\ldots N}$ as the sampling data of the adaptive fGPm, where $x_{(1)} \leq x_{(2)} \leq \cdots \leq x_{(N)}$ and so on, in ascending order of the statistical data.

Step 2: Calculate the mean of the sequence μ using Equation (17).

$$\mu = \frac{1}{N}\sum_{i=1}^{N} x_i \tag{17}$$

Step 3: Assume that the random variable, from which all sample sequences $x_i|_{i=1\ldots N}$ are individually drawn, has a probability density function that is a complex function related to θ. The log-likelihood function for parameters α and δ is then given by Equation (20).

$$L^*(\theta) = -\log 2 - N - \sum_{i=1}^{N} \log(1-\theta x_i) - N \log\left[-\frac{1}{N\theta}\sum_{i=1}^{N} \log(1-\theta x_i)\right] \tag{18}$$

Step 4: When $\theta < 1/x_{(N)}$, the local maximum value $\hat{\theta}$ is computed using the method of maximum likelihood estimation, yielding the following maximum likelihood estimates:

$$\hat{\theta} = \underset{\mu}{\operatorname{argmax}} L^*(\theta \mid x_i) \tag{19}$$

The maximum likelihood estimate for α is:

$$\hat{a} = -N\sum_{i=1}^{N}\log(1-\hat{\theta}x_i) \tag{20}$$

The maximum likelihood estimate for δ is:

$$\hat{\delta} = \frac{2}{\hat{a}\hat{\theta}} \tag{21}$$

5. Experimental Cases and Analysis

5.1. Data Description

To validate the effectiveness of the adaptive fGPm proposed in this paper for short-term wind power forecasting, a wind power dataset from a wind farm in Northwest China was selected for analysis. The data spans from 1 October 2019, 00:00 to 25 December 2019, 23:45, with a sampling frequency of 30 times per minute. The dataset includes meteorological characteristics and corresponding power data, comprising local temperature, air humidity, atmospheric pressure, wind speed, and direction. By employing OMI-Coherence analysis, numerical weather prediction (NWP) data strongly correlated with wind power output were selected as model inputs. The forecasting target is set for wind power within the next 6 to 24 h, predicted on an hourly average basis. The forecasting model integrates the NWP data from the previous four days, historical power data, and one-day-ahead NWP forecasts to predict the trend of wind power within the next 24 h.

5.2. Experimental Process

Due to the variability of wind speed, there is an inherent uncertainty in wind power generation. This experiment selects two seasons with different meteorological characteristics for study: one with high fluctuation in winter and another with relatively stable conditions in summer. Specifically, Case One involves data from 1 December 2019, 7:00 to 11 December 2019, 18:00, as shown in Figure 4, totaling 132 data points as the subject of study.

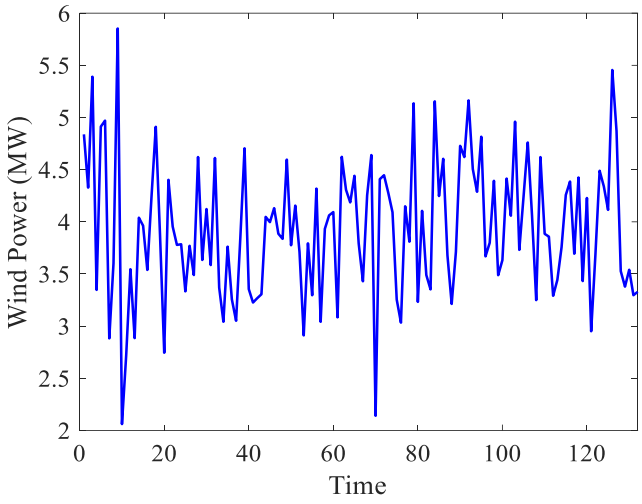

Figure 4. Original Wind Power Data.

Before using the adaptive fGPm iterative model for prediction, it is first confirmed whether the selected wind power sequence possesses LRD, ensuring the systematic and scientific nature of the research. The overall experimental procedure is depicted in Figure 5.

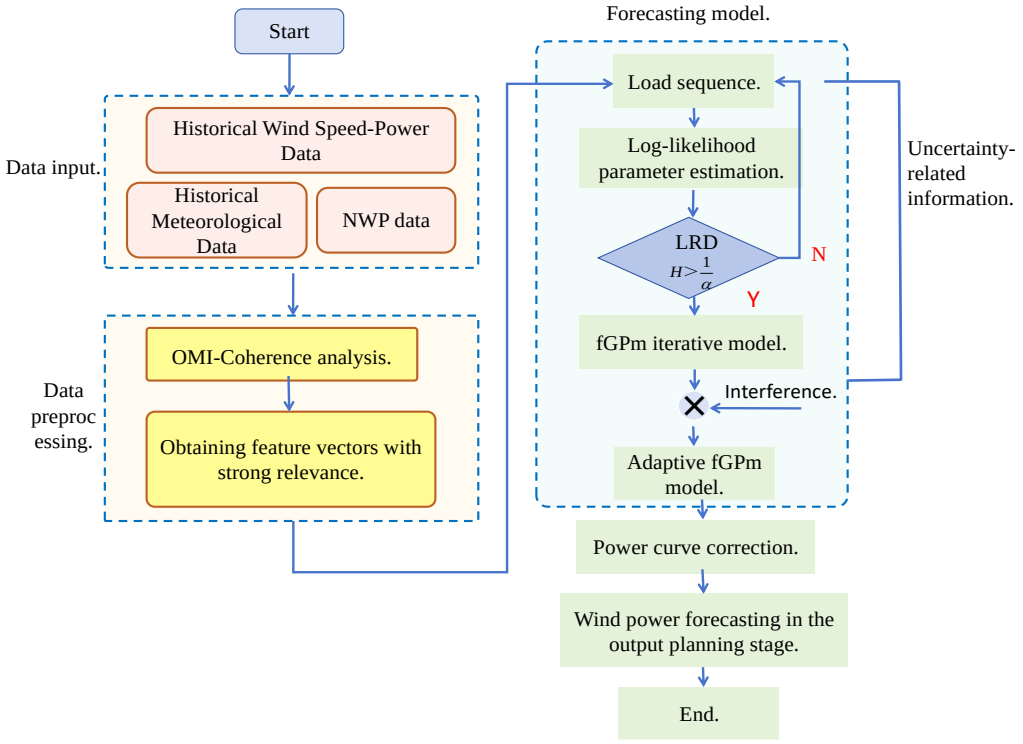

Figure 5. Wind farm power generation forecasting model framework.

As shown in Figure 5, detailed preprocessing of the historical operation data from the wind farm was first carried out, including the removal of outliers and effective imputation of missing values. Given the coupling between features in the original dataset, before feature extraction and reconstruction, this study applied the OMI-Coherence method to accurately capture the correlations between meteorological features and power generation. The results indicate that wind speed, wind direction, humidity, temperature, atmospheric pressure, and air density have correlation coefficients with power generation of 0.6808, 0.6267, 0.6426, 0.4645, 0.2763, and 0.1939, respectively. To efficiently extract pivotal features and reduce the model's input dimensionality, this study selected wind direction and speed, which have a strong association with power output—as the input features for the NWP model, thereby constructing a data sequence with significant predictive value. Subsequently, the study employed an improved maximum likelihood estimation method to precisely estimate the parameters of the wind farm forecasting model, with detailed estimation results presented in Table 1. Based on the condition $H > 1/\alpha$, the Hurst indices for the two data ensembles were determined to be 0.8315 and 0.7915, both exceeding the threshold of 0.5, thereby satisfying the criteria for LRD.

Table 1. Forecasting Model Parameter Estimation.

	H	α	$\hat{\mu}$	$\hat{\delta}$
Case 1	0.8315	1.7142	640.2534	3.1201
Case 2	0.7915	1.7235	750.4211	2.6617

The key parameter estimates shown in Table 1 include H, shape parameter α, location parameter $\hat{\mu}$, and diffusion parameter $\hat{\delta}$. Specifically, the H reveals the LRD characteristic of wind power time series. Higher H values (such as 0.8315 in Case 1 and 0.7915 in Case 2) indicate a significant persistence in trends, suggesting that historical patterns in wind power output have a substantial influence on future predictions. The α represents the tail behavior of the data distribution, with higher α values (1.7142 in Case 1 and 1.7235 in Case 2) reflecting heavy-tailed characteristics, which help the model respond to large fluctuations in wind power caused by environmental changes, enhancing its ability to handle extreme events.

The $\hat{\mu}$ (640.2534 in Case 1 and 750.4211 in Case 2) indicates the central tendency of wind power output, reflecting typical power output levels across different seasons.

To address the uncertainties inherent in wind power forecasting, $\hat{\delta}$ was introduced to simulate disturbances, such as meteorological fluctuations, wind speed variations, and environmental changes, which can lead to deviations in forecasted values. This parameter enables adaptive adjustments according to actual observed values, allowing the model to respond dynamically to these disturbances. The $\hat{\delta}$ results ($\hat{\delta}$ = 3.1201 in Case 1 and $\hat{\delta}$ = 2.6617 in Case 2) reflect the model's flexibility in adapting to different levels of environmental variability, with higher values indicating a greater responsiveness to fluctuations.

By incorporating these interference factors, the model improves its robustness and accuracy in forecasting wind power trends. This approach not only substantiates the scientific validity of utilizing the adaptive fGPm forecasting model for model construction but also provides a solid foundation for setting the parameters effectively in the wind power trend forecasting model.

5.3. Prediction Results

5.3.1. Case 1: Winter

Utilizing the NWP feature values and power data extracted from 1 December 2019, at 07:00 to 11 December 2019, at 18:00 during the winter season as the input sequence, the NWP data for the forthcoming day is employed as historical data to forecast the 12th, 24th, 36th, and 48th wind power values for the subsequent day. Figure 6 illustrates the wind power forecast curve, derived from the adaptive fGPm-based iterative differential prediction model, juxtaposing the predicted and actual wind power values.

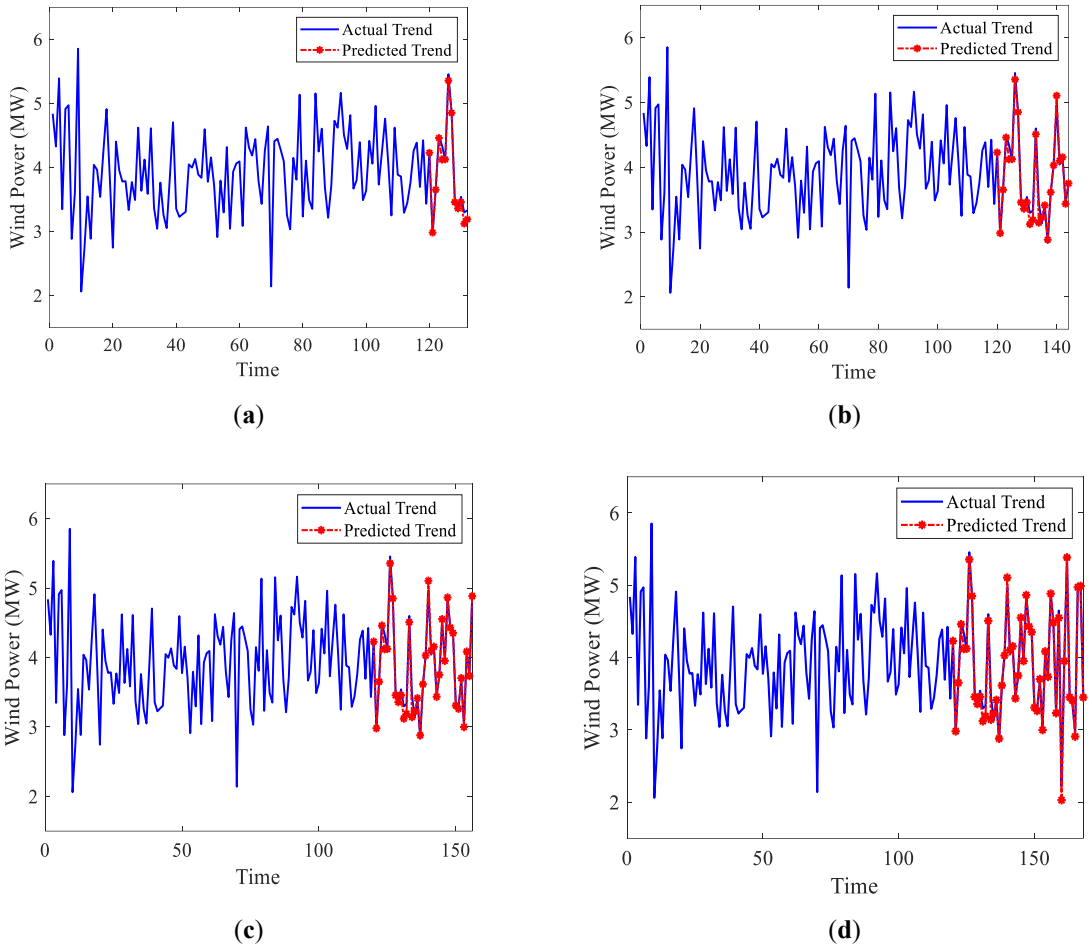

Figure 6. Winter Wind Power Forecasting Results for Wind Turbine Generators; (**a**) predicting 12 steps; (**b**) predicting 24 steps; (**c**) predicting 36 steps; (**d**) predicting 48 steps.

5.3.2. Case 2: Summer

The NWP data and power data from 1 July 2019, 7:00 a.m. to 12 July 2019, 6:00 p.m., along with the NWP data for the following day, were used as historical data. The adaptive fGPm-based iterative differential forecasting model was then applied to predict 12, 24, 36, and 48 wind power values for the next day, as shown in Figure 7.

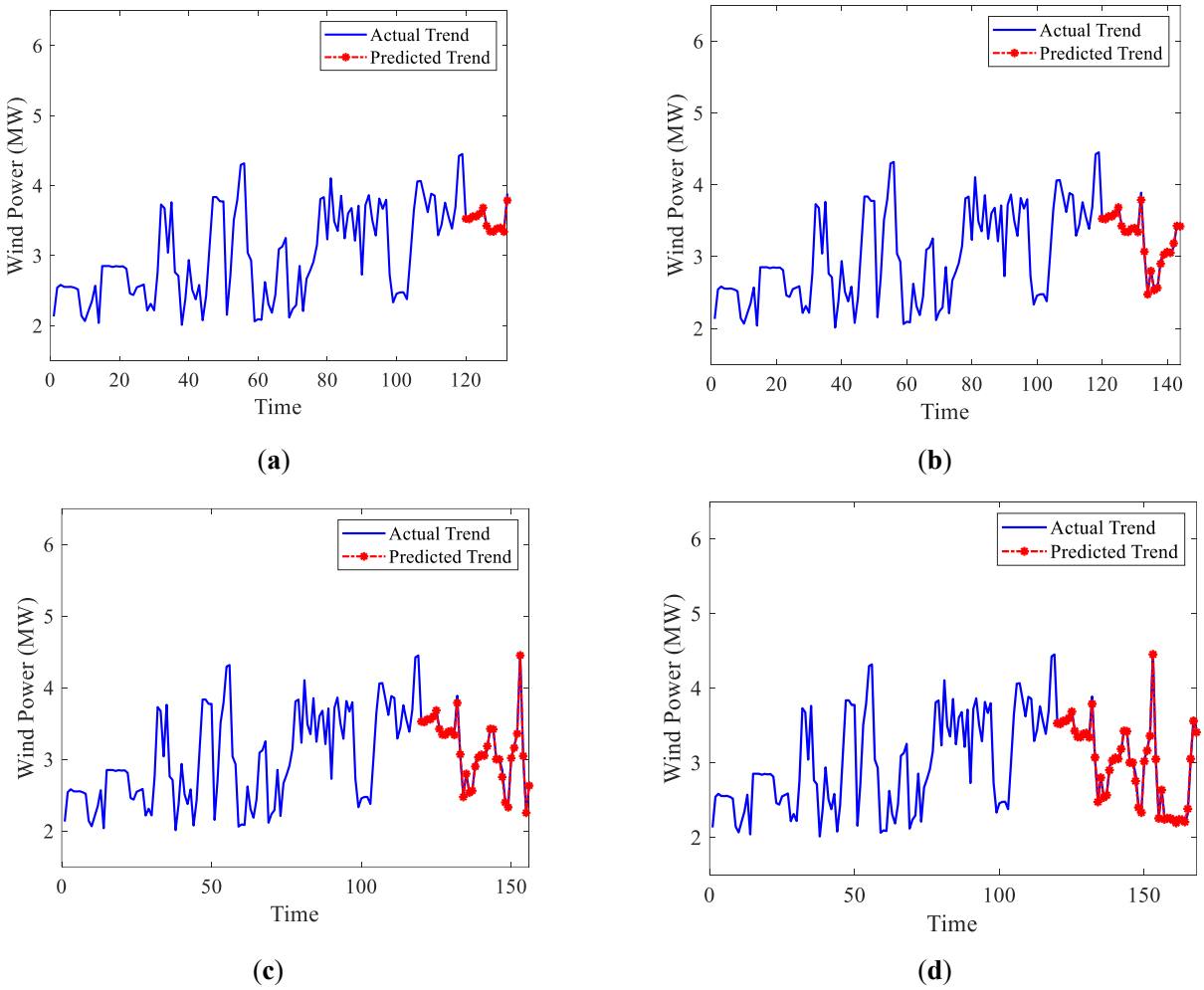

Figure 7. Summer Wind Power Forecasting Results for Wind Turbine Generators; (**a**) predicting 12 steps; (**b**) predicting 24 steps; (**c**) predicting 36 steps; (**d**) predicting 48 steps.

In Figure 7, the predicted values are shown alongside the actual observed wind power data. The comparison demonstrates that the adaptive fGPm model accurately captures short-term fluctuations in wind power, particularly over the initial forecast periods (12 and 24 h). The model is able to closely mirror actual power output, reflecting its robustness in adapting to observed values. However, as the forecasted period extends to 36 and 48 h, the model's accuracy begins to decline. This trend is expected, given the inherent uncertainty in wind power predictions, as the further ahead the prediction, the more susceptible it is to errors arising from factors such as sudden wind direction changes, weather system dynamics, and real-time environmental changes.

Figures 6 and 7 distinctly demonstrate the precision of the adaptive fGPm iterative differential forecasting model in capturing the short-term trends in wind power output for wind turbines. Comparative analysis of the model's forecasts against actual wind power data reveals improved accuracy. Nonetheless, it is observed that the accuracy of wind power trend predictions for the same sequence of samples decreases as the forecasted period extends.

5.4. Model Performance Analysis

To comprehensively evaluate the forecasting accuracy of the adaptive fGPm-based iterative differential prediction model, this paper selects the Root Mean Square Error (RMSE), Mean Absolute Percentage Error (MAPE), and the Coefficient of Determination (R-squared, R^2) as metrics for assessing the precision of the final point forecasts. The calculation formulas are as follows:

$$\mathrm{RMSE} = \sqrt{\frac{1}{N}\sum_{i=1}^{N}\left(\frac{y_i - \hat{y}_i}{y_{\mathrm{cap}}}\right)^2} \tag{22}$$

$$\mathrm{MAPE} = \frac{100\%}{N}\sum_{i=1}^{N}\left|\frac{\hat{y}_i - y_i}{y_i}\right| \tag{23}$$

$$R^2 = \frac{\sum_{i=1}^{N}\left[(y_i - \overline{y_i})(\hat{y}_i - \overline{y}_i)\right]}{\sum_{i=1}^{N}(y_i - \overline{y_i})^2 \sum_{i=1}^{N}\left(\hat{y}_i - \overline{\hat{y}_i}\right)^2} \tag{24}$$

In Equations (22)–(24), y_i and $\hat{y}_i$ represent the actual and forecasted power at time instance i, respectively; $\overline{y_i}$ and $\overline{\hat{y}_i}$ denote the mean values of the actual and forecasted powers, respectively; N is the number of samples; and y_{cap} signifies the installed capacity.

Error Analysis from Table 2 Leads to the Following Conclusions:

(1) RMSE and MAPE: The data in the table reveal that, overall, the RMSE and MAPE values for winter are significantly higher than those for summer, indicating higher forecasting accuracy during the relatively stable wind speeds of summer. Concurrently, within the same season, as the forecast length increases, the RMSE and MAPE values gradually increase, yet maintain relatively small means. This suggests that, although winter forecasting errors may exhibit larger fluctuations in some cases, the general level remains acceptably low.

(2) R^2: Utilizing the coefficient of determination to assess the final forecast results, the values for summer are notably higher than those for winter. This indicates a greater fit, with the independent variables explaining the dependent variable to a higher degree, thereby signifying a more valuable reference for the forecasting model.

Table 2. Forecast Model Performance Analysis.

Season	Forecast Length	Evaluation Metrics		
		RMSE(MW)	**MAPE(%)**	R^2
Winter	12	0.842	22.456	0.9614
	24	1.014	23.412	0.9721
	36	1.021	25.321	0.9717
	48	1.332	26.334	0.9711
Summer	12	0.772	5.047	0.9750
	24	0.956	5.678	0.9711
	36	1.121	6.123	0.9817
	48	1.242	7.123	0.9830

In summary, the adaptive fGPm iterative differential model has demonstrated a certain level of effectiveness in wind power trend forecasting. In practical applications, when selecting the forecast length, it is necessary to make flexible trade-offs based on specific requirements to achieve an optimal balance.

5.5. Comparison of Different Models

5.5.1. Comparative Analysis of Model Prediction Result

To substantiate the superior predictive accuracy of the proposed model, it was compared with the adaptive fGPm and CNN-GRU models. Historical data, including NWP and power output data, were collected on 26 December 2019 (winter), from 7:00 to 19:00, and on 12 July 2019 (summer), during the same hours. Samples were taken every 30 min to forecast the wind power output for intervals of 6, 12, 18, and 24 h ahead. The comparative results are depicted in Figures 8 and 9.

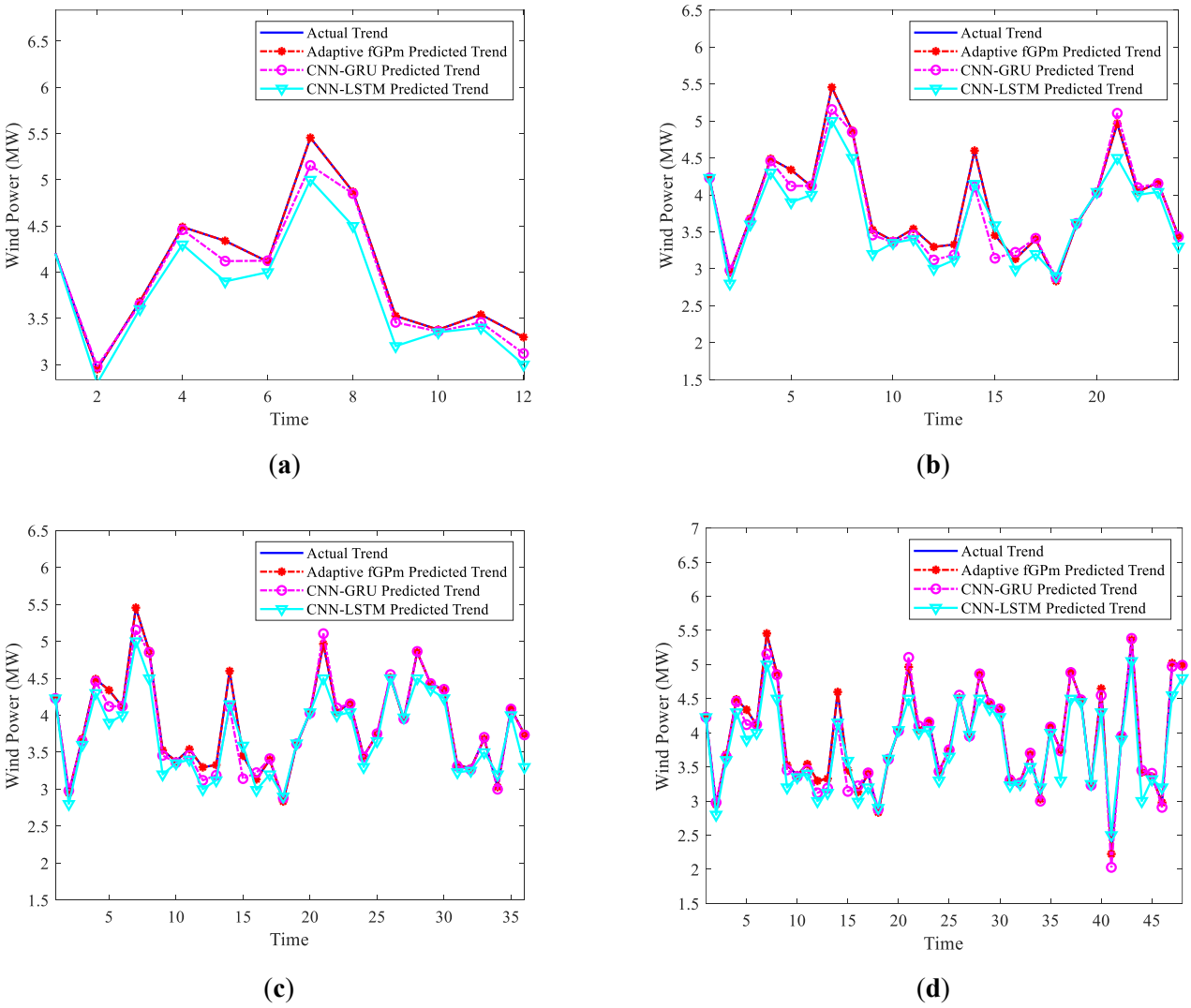

Figure 8. Comparison of Prediction Curves from Different Models in Winter. (**a**) 6 h (**b**) 12 h (**c**) 18 h (**d**) 24 h.

The comparative analysis from Figures 8 and 9 reveals that the power output of wind farms is generally higher in winter than in summer. This phenomenon can likely be attributed to the greater variability in wind speed during the winter months, which in turn leads to a significant increase in the volatility of wind power output. All models have demonstrated a satisfactory fit in simulating the actual wind power curves. However, when confronted with sampling points where there are sharp changes in wind speed, the adaptive fGPm model proposed in this study, with its capability to capture long-range dependencies, shows a notably significant advantage in predictive accuracy. By conducting an in-depth analysis of the data, this model significantly enhances the consistency between predicted and observed values, achieving a high degree of accuracy in fitting the wind

power curve. In contrast, the CNN-LSTM model exhibits relatively larger predictive errors at some sampling points, indicating a potential need for further optimization in handling such extreme fluctuations. This refined translation maintains the original message's intent while enhancing the language for a professional and academic context.

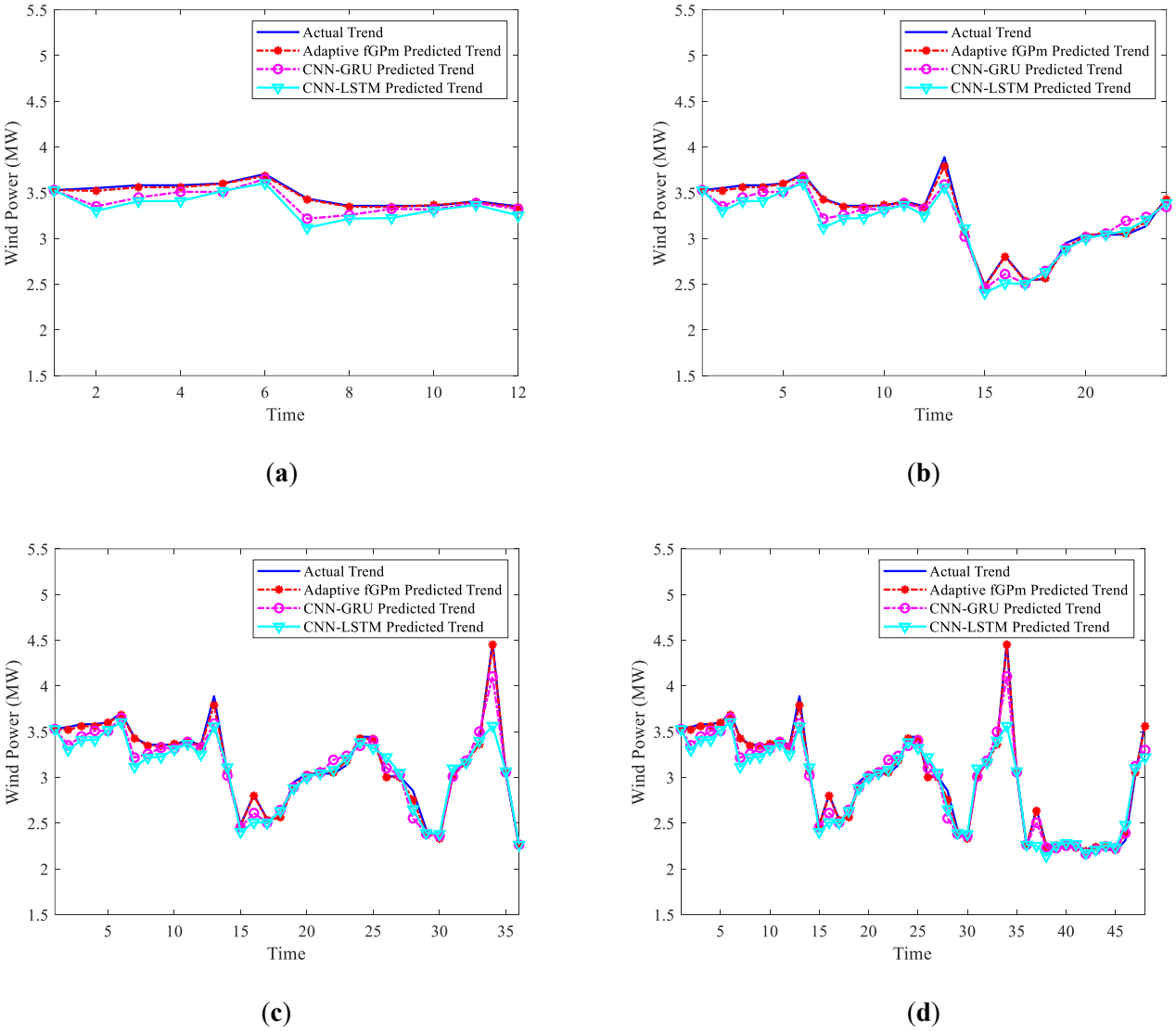

Figure 9. Comparison of Prediction Curves from Different Models in Summer. (**a**) 6 h (**b**) 12 h (**c**) 18 h (**d**) 24 h.

5.5.2. Performance Comparison of Different Models

In the performance comparison of various models, the evaluative indicators presented in Table 3 indicate that the Adaptive fGPm model demonstrates superior performance over the CNN-GRU and CNN-LSTM models in two pivotal metrics: RMSE and MAPE. The RMSE of the Adaptive fGPm model exhibits an average decrease of 0.448 MW and 0.466 MW relative to the CNN-GRU and CNN-LSTM models, respectively. Additionally, the MAPE has seen an average reduction of 6.936% and 9.702%, respectively. This significant improvement in performance is mainly due to two key aspects: First, the model's adaptive drift coefficient dynamically adjusts to incoming data, more accurately reflecting the trends in wind power variations. Second, by effectively harnessing the LRD features of time series data, the model distills overall characteristics and accentuates the importance of critical input information, which substantially improves the precision of the forecasts.

Table 3. Comparative Analysis of Forecasting Results Across Various Models.

Season	Prediction Time	CNN-GRU			CNN-LSTM			Adaptive fGPm		
		RMSE(MW)	MAPE(%)	R^2	RMSE(MW)	MAPE(%)	R^2	RMSE(MW)	MAPE(%)	R^2
Winter	6 h	0.887	30.321	0.9421	1.223	37.125	0.9212	0.505	19.231	0.9678
	12 h	0.997	31.151	0.9511	1.321	38.243	0.9328	0.609	20.421	0.9720
	18 h	1.552	32.321	0.9624	1.421	39.354	0.9427	0.891	21.504	0.9812
	24 h	1.921	33.256	0.9725	1.521	40.321	0.9578	0.997	22.022	0.9878
Summer	6 h	0.778	7.126	0.9510	0.899	8.121	0.9312	0.231	5.231	0.9895
	12 h	0.887	8.326	0.9623	0.951	8.231	0.9427	0.401	4.355	0.9778
	18 h	0.901	8.541	0.9711	0.996	9.332	0.9513	0.586	5.501	0.9895
	24 h	0.998	9.231	0.9778	1.211	9.512	0.9620	0.799	6.521	0.9955
Average		1.115	20.034	0.9613	1.193	23.800	0.9427	0.627	13.098	0.9826

Table 3 also shows the R^2 values, which reflect the predictive accuracy of the models. The CNN-GRU model has an average R^2 value of 0.9613, indicating strong predictive capability. The CNN-LSTM model has an average R^2 value of 0.9427, slightly lower than CNN-GRU but still shows good performance. The Adaptive fGPm model outperforms both, with an average R^2 value of 0.9705, demonstrating superior accuracy and stability in wind power forecasting. This suggests that the Adaptive fGPm model is better at capturing the dynamic trends in wind power data, which contributes to its overall higher prediction accuracy.

6. Conclusions

The adaptive fGPm iterative differential forecasting method proposed in this study demonstrates superior performance and high accuracy in short-term wind power forecasting, showcasing significant practical application potential. The main conclusions are as follows:

Key Role of Data Processing: To address the impact of the complex temporal characteristics of wind power generation on model accuracy, we employed the Orthogonalized Maximum Information Coefficient feature selection method. This significantly enhanced the correlation between wind power and the selected features, validating the effectiveness of the feature extraction approach.

LRD Characteristics of Wind Power Series: By analyzing the relationship between the Hurst parameter and feature indices, we revealed the LRD characteristics of wind power series. This finding provides a theoretical basis for modeling with the adaptive fGPm, particularly improving trend prediction accuracy under optimized sample lengths and forecasting horizons.

Parameter Estimation of New Feature Function Method: We successfully applied a new feature function method to estimate parameters such as stability index, skewness index, drift coefficient, and diffusion parameter within the adaptive fGPm model, laying a solid foundation for building a reliable forecasting model.

Superiority of the Adaptive fGPm Forecasting Model: The adaptive fGPm iterative differential forecasting model effectively addresses uncertainties in wind power generation by introducing tail parameters, thereby enhancing the flexibility of LRD characterization. This model demonstrated advantages in forecasting high-volatility data, with its diffusion coefficient adapting to environmental changes to more accurately reflect dynamic wind power characteristics.

Comparison with Other Models: Comparative analyses with mainstream forecasting models such as CNN-GRU and CNN-LSTM demonstrated the superiority and versatility of the adaptive fGPm model in describing wind power data, achieving higher prediction accuracy.

In summary, This research provides an innovative adaptive fGPm iterative differential forecasting model for accurate short-term wind power predictions, aiding power departments in optimizing generation planning and scheduling. Furthermore, it serves as an effective reference for other time series forecasting scenarios, such as wind speed, photovoltaic generation, and precipitation.

Author Contributions: F.C.: conceptualization, methodology, software, writing—original draft. writing—review and editing, methodology. T.Z.: formal analysis, data curation. Y.J.: Project administration, Resources, Supervision. D.C.: Funding acquisition, Supervision, Software. All authors have read and agreed to the published version of the manuscript.

Funding: This work was supported by the Science and Technology Project of Quanzhou City under Grant 2024QZC004R, and the Natural Science Foundation of Fujian Province under Grant 2024J01208. and the Science and Technology Project of Fujian Province under Grant 2023H6026.

Data Availability Statement: Wind farms have confidentiality requirements regarding their data and we cannot publish the data we have used.

Acknowledgments: The authors would like to thank the anonymous reviewers who gave valuable suggestions that have helped to improve the quality of the manuscript.

Conflicts of Interest: The authors declare no conflicts of interest.

References

1. Li, Y.; Sun, C.; Jiang, Y.; Feng, F. Scaling Method of the Rotating Blade of a Wind Turbine for a Rime Ice Wind Tunnel Test. *Energies* **2019**, *12*, 627. [CrossRef]
2. Thango, B.A.; Bokoro, P.N. Prediction of the Degree of Polymerization in Transformer Cellulose Insulation Using the Feedforward Backpropagation Artificial Neural Network. *Energies* **2022**, *15*, 4209. [CrossRef]
3. Faheem, M.; Al-Khasawneh, M.A.; Khan, A.A.; Madni, S.H.H. Cyberattack patterns in blockchain-based communication networks for distributed renewable energy systems: A study on big datasets. *Data Brief* **2024**, *42*, 110212. [CrossRef] [PubMed]
4. Faheem, M.; Al-Khasawneh, M.A. Multilayer cyberattacks identification and classification using machine learning in internet of blockchain (IoBC)-based energy networks. *Data Brief* **2024**, *42*, 110461. [CrossRef] [PubMed]
5. Zhao, P.F.; Hu, W.H.; Cao, D.; Zhang, Z.Y.; Liao, W.L.; Chen, Z.; Huang, Q. Enhancing multivariate, multi-step residential load forecasting with spatiotemporal graph attention-enabled transformer. *Int. J. Electr. Power Energy Syst.* **2024**, *160*, 110074. [CrossRef]
6. Zhang, Y.; Kong, X.; Wang, J.; Wang, H.; Cheng, X. Wind power forecasting system with data enhancement and algorithm improvement. *Renew. Sustain. Energy Rev.* **2024**, *196*, 114349. [CrossRef]
7. Ju, Y.; Sun, Y.; Chen, Q. A model combining convolutional neural network and LightGBM algorithm for ultra-short-term wind power forecasting. *IEEE Access* **2019**, *7*, 28309–28318. [CrossRef]
8. Zhao, Y.B.; Guo, N.; Chen, W. Multi-step ahead forecasting for electric power load using an ensemble model. *Expert Syst. Appl.* **2023**, *211*, 118649. [CrossRef]
9. Li, Y.; Wu, Z.; Su, Y. Adaptive Short-term Wind Power Forecasting Based on Feature Extraction and Fuzzy Gaussian Process Regression. *Renew. Energy* **2023**, *217*, 119146. [CrossRef]
10. Cai, H.; Jia, X.; Feng, J. A combined filtering strategy for short term and long term wind speed prediction with improved accuracy. *Renew. Energy* **2019**, *136*, 1082–1090. [CrossRef]
11. Wang, J.; Tang, X.D. An intensive decomposition integration paradigm for short-term wind power forecasting based on feature extraction and optimal weighted combination strategy. *Measurement* **2023**, *223*, 113811. [CrossRef]
12. Lu, P.; Ye, L.; Pei, M.; Zhao, Y.N. Short-term wind power forecasting based on meteorological feature extraction and optimization strategy. *Renew. Energy* **2022**, *184*, 642–661. [CrossRef]
13. Liao, S.; Tian, X.; Liu, B.; Liu, T.; Su, H.; Zhou, B. Short-Term Wind Power Prediction Based on LightGBM and Meteorological Reanalysis. *Energies* **2022**, *15*, 6287. [CrossRef]
14. Wang, Y.S.; Gao, J.; Xu, Z.W.; Luo, J.D.; Li, L.X. A Prediction Model for Ultra-Short-Term Output Power of Wind Farms Based on Deep Learning. *Int. J. Comput. Commun.* **2020**, *15*, 3901. [CrossRef]
15. Sun, Z.X.; Zhao, M.Y. Short-term wind power forecasting based on VMD decomposition, ConvLSTM networks and error analysis. *IEEE Access* **2020**, *8*, 134422–134434. [CrossRef]
16. Lu, P. Feature extraction of meteorological factors for wind power prediction based on variable weight combined method. *Renew. Energy* **2021**, *179*, 1925–1939. [CrossRef]
17. Yang, G.H.; Qi, X.; Jia, R.; Liu, Y.F.; Meng, F.; Ma, X.; Xing, X.W. Short-term wind power prediction based on CEEMD-SE, CNN&LSTM-GRU. *Electr. Power* **2024**, *57*, 55–61.
18. Ji, J.; Wang, D.; Xu, D.; Xu, C. Combining a self-exciting point process with the truncated generalized Pareto distribution: An extreme risk analysis under price limits. *J. Empir. Financ.* **2020**, *57*, 52–70. [CrossRef]
19. Lahiri, S.N.; Das, U.; Nordman, D.J. Empirical Likelihood for a Long Range Dependent Process Subordinated to a Gaussian Process. *J. Time Ser. Anal.* **2019**, *40*, 447–466. [CrossRef]
20. Ye, L.; Li, Y.L.; Pei, M.; Zhao, Y.N.; Li, Z.; Lu, P. A novel integrated method for short-term wind power forecasting based on fluctuation clustering and history matching. *Appl. Energy* **2022**, *327*, 120131. [CrossRef]
21. Wu, Y.K. Deterministic and probabilistic wind power forecasts by considering various atmospheric models and feature engineering approaches. *IEEE Trans. Ind. Appl.* **2022**, *59*, 192–206. [CrossRef]

22. Noorollahi, Y.; Mohammad, A.J.; Ahmad, K. Using artificial neural networks for temporal and spatial wind speed forecasting in Iran. *Energy Convers. Manag.* **2016**, *115*, 17–25. [CrossRef]
23. Chen, Y.J.; Xiao, J.W.; Wang, Y.W.; Li, Y. Regional wind-photovoltaic combined power generation forecasting based on a novel multi-task learning framework and TPA-LSTM. *Energy Convers. Manag.* **2023**, *297*, 117715. [CrossRef]
24. Razin, A.; Victor, S.; Roberto, T.; Amitava, D.; Muammer, D.A. Computationally expedient Photovoltaic power Forecasting: A LSTM ensemble method augmented with adaptive weighting and data segmentation technique. *Energy Convers. Manag.* **2022**, *258*, 115563. [CrossRef]
25. Ali, A.; Ahmed, A.; Moussa, L.; Yassine, E.H. Short-term self consumption PV plant power production forecasts based on hybrid CNN-LSTM, ConvLSTM models. *Renew. Energy* **2021**, *177*, 101–112.
26. Zhang, W.; Cai, Y.; Zhan, H.Y.; Yang, M.; Zhang, W. Multi-energy load forecasting for small-sample integrated energy systems based on neural network Gaussian process and multi-task learning. *Energy Convers. Manag.* **2024**, *321*, 119027. [CrossRef]
27. Li, C.; Li, G.J.; Wang, K.Y.; Han, B. A multi-energy load forecasting method based on parallel architecture CNN-GRU and transfer learning for data deficient integrated energy systems. *Energy* **2022**, *259*, 124967. [CrossRef]
28. Ge, R.; Zhou, M.; Luo, Y. McTwo: A two-step feature selection algorithm based on maximal information coefficient. *BMC Bioinform.* **2016**, *17*, 142. [CrossRef]
29. Han, Y.; Mi, L.H.; Shen, L.; Cai, C.S.; Liu, Y.C.; Li, K.; Xu, G.J. A short-term wind speed prediction method utilizing novel hybrid deep learning algorithms to correct numerical weather forecasting. *Appl. Energy* **2022**, *312*, 118777. [CrossRef]
30. Marquardt, T. Fractional Lévy processes with an application to long memory moving average processes. *Bernoulli* **2006**, *12*, 1099–1126. [CrossRef]
31. Chen, J.; Liu, H.; Chen, C.; Zhu, D. Wind speed forecasting using multi-scale feature adaptive extraction ensemble model with error regression correction. *Expert Syst. Appl.* **2022**, *207*, 117358. [CrossRef]
32. Lim, S.; Li, M. A generalized Cauchy process and its application to relaxation phenomena. *J. Phys. A Math. Gen.* **2006**, *39*, 2935–2951. [CrossRef]
33. Li, M.; Li, J.Y. Generalized Cauchy model of sea level fluctuations with long-range dependence. *Phys. A Stat. Mech. Its Appl.* **2017**, *484*, 309–335. [CrossRef]
34. Dou, C.; Zheng, Y.; Yue, D.; Zhang, Z.; Ma, K. Hybrid model for renewable energy and loads prediction based on data mining and variational mode decomposition. *IET Gener Transm. Distrib.* **2018**, *12*, 2642–2649. [CrossRef]
35. Cao, B.; Chang, L. Development of Short-Term Wind Power Forecasting Methods. In Proceedings of the 2022 IEEE 7th Southern Power Electronics Conference (SPEC), Nadi, Fiji, 5–8 December 2022; pp. 1–5. [CrossRef]
36. Feng, C.; Cui, M.; Hodge, B.M.; Zhang, J. A data-driven multi-model methodology with deep feature selection for short-term wind forecasting. *Appl. Energy* **2017**, *190*, 1245–1257. [CrossRef]
37. Kisvari, A.; Lin, Z.; Liu, X. Wind power forecasting-a data-driven method along with gated recurrent neural network. *Renew. Energy* **2021**, *163*, 1895–1909. [CrossRef]
38. Li, L.; Zhang, Z.; Zhang, S. Hybrid algorithm based on content and collaborative filtering in recommendation system optimization and simulation. *Sci. Progr.* **2021**, *2021*, 7427409. [CrossRef]
39. Yang, Z.; Zhou, F.; Yang, L.; Zhang, Q. A new prediction method for recommendation system based on sampling reconstruction of signal on graph. *Expert Syst. Appl.* **2020**, *159*, 113587. [CrossRef]
40. Carrillo, R.E.; Aysal, T.C.; Barner, K.E. A generalized Cauchy distribution framework for problems requiring robust behavior. *EURASIP J. Adv. Signal Process.* **2010**, *2010*, 312989. [CrossRef]
41. Liu, H.; Song, W.; Zio, E. Generalized Cauchy difference iterative forecasting model for wind speed based on fractal time series. *Nonlinear Dyn.* **2021**, *103*, 759–773. [CrossRef]
42. Liu, H.; Song, W.Q.; Zio, E. Fractional Lévy stable motion with LRD for RUL and reliability analysis of li-ion battery. *ISA Trans.* **2022**, *125*, 360–370. [CrossRef] [PubMed]
43. Kogon, S.M.; Manolakis, D.G. Signal modeling with self-similar α -stable processes: The fractional levy stable motion model. *IEEE Trans. Signal Process.* **1996**, *44*, 1006–1010. [CrossRef]
44. Song, W.; Liu, H.; Zio, E. Long-range dependence and heavy tail characteristics for remaining useful life prediction in rolling bearing degradation. *Appl. Math. Model.* **2022**, *102*, 268–284. [CrossRef]
45. Song, W.Q.; Duan, S.W.; Chen, D.D.; Zio, E.; Yan, W.D.; Cai, F. Finite Iterative Forecasting Model Based on Fractional Generalized Pareto Motion. *Fractal Fract.* **2022**, *6*, 471. [CrossRef]
46. Ramirez, J.A.; Echeverria, J.C.; Rodriguez, E. Performance of a high-dimensional R/S method for Hurst exponent estimation. *Phys. A Stat. Mech. Its Appl.* **2008**, *387*, 6452–6462. [CrossRef]
47. Jie, X.; Song, W.Q.; Francesco, V. Generalized Cauchy Process: Difference Iterative Forecasting Model. *Fractal Fract.* **2021**, *5*, 38. [CrossRef]
48. Savović, S.; Djordjevich, A. Investigation of Mode Coupling in Graded Index Plastic Optical Fibers Using the Langevin Equation. *J. Light. Technol.* **2020**, *38*, 6644–6647. [CrossRef]
49. Sayah, M.; Guebli, D.; Masry, Z.A.; Zerhoui, N. Robustness testing framework for RUL prediction Deep LSTM networks. *ISA Trans.* **2021**, *113*, 28–38. [CrossRef]
50. Wang, Y.; Zou, R.; Liu, F.; Zhang, L.J.; Liu, Q.Y. A review of wind speed and wind power forecasting with deep neural networks. *Appl. Energy* **2021**, *304*, 117766. [CrossRef]

51. Zheng, J.; Du, J.; Wang, B.; Klemeš, J.J.; Liao, Q.; Liang, Y. A hybrid framework for forecasting power generation of multiple renewable energy sources. *Renew. Sustain. Energy Rev.* **2023**, *172*, 113046. [CrossRef]
52. Zhang, J.H.; Yan, J.; Liu, Y.Q.; Lin, F.S. Short-term forecasting and uncertainty analysis of wind turbine power based on long short-term memory network and Gaussian mixture model. *Appl. Energy* **2019**, *241*, 229–244. [CrossRef]
53. Jiang, M.; He, Y.; Zhang, T.; Yang, B. Wind Power Prediction Based on Feature Selection and Error Correction. *Distrib. Energy* **2023**, *8*, 37–43. [CrossRef]
54. Ma, Z.; Zhang, L.; Ba, Y.; Xie, M.; Zhang, P.; Wang, X. Ultra-Short-Term Wind Power Prediction Based on Adaptive Quadratic Mode Decomposition and CNN-BiLSTM. *Sol. Energy* **2024**, *45*, 429–435. [CrossRef]
55. Chen, Y.; Li, Y.; Li, H. Ultra-Short-Term Prediction of Wind Power Based on VMD-PE-MulitiBiLSTM. *Distrib. Energy* **2024**, *9*, 1–7. [CrossRef]
56. Wu, X.; Liang, X.; Zhu, H.; Zhang, D. Short-term Wind Power Prediction Based on CEEMDAN-GRA-PCC-ATCN. *J. Guangxi Univ. (Eng. Ed.)* **2022**, *52*, 146–156.
57. Liu, J.J.; Wang, J.Z.; Niu, Y.B.; Ji, B.Q.; Gu, L. A point-interval wind speed forecasting system based on fuzzy theory and neural networks architecture searching strategy. *Eng. Appl. Artif. Intell.* **2024**, *132*, 107906. [CrossRef]
58. Hodge, B.M.; Zeiler, A.; Brooks, D.C.; Blau, G.; Joseph, P.; Gintaras, R. Improved Wind Power Forecasting with ARIMA Models. *Comput. Aided Chem. Eng.* **2011**, *29*, 1789–1793. [CrossRef]